JACS Au
AN OPEN ACCESS JOURNAL OF THE AMERICAN CHEMICAL SOCIETY

pubs.acs.org/jacsau
Article

Antarmycins: Discovery, Biosynthesis, Anti-pathogenic Bacterial Activity, and Mechanism of Action from Deep-Sea-Derived *Pseudonocardia antarctica*

Zhenbin Zhou, Jiafan Yang, Junying Ma, Zhuo Shang, Runping Fang, Xinpeng Tian, Qinglian Li,* and Jianhua Ju*

Cite This: *JACS Au* 2025, 5, 237−249
Read Online
ACCESS | Metrics & More | Article Recommendations | Supporting Information

ABSTRACT: The rapid emergence of antimicrobial-resistant pathogenic microbes has accelerated the search for novel therapeutic agents. Here we report the discovery of antarmycin A (**1**), an antibiotic containing a symmetric 16-membered macrodiolide core with two pendant vancosamine moieties, one of which is glucosylated, from deep-sea-derived *Pseudonocardia antarctica* SCSIO 07407. The biosynthetic gene cluster of **1** was identified on a giant plasmid featuring transferable elements. In-depth biosynthetic investigation enabled us to (i) identify a set of seven genes associated with the product of the vancosamine moiety; (ii) discover two glycosyltransferases dedicated to the transfer of pendant sugars; and (iii) isolate rhamnose-modified antarmycin B (**2**) and a deglucosylated derivative antarmycin C (**3**) from genetically engineered mutant strains. Antibacterial assays revealed that **1** displays superior antibacterial properties with potent *in vitro* activities against the critical priority pathogens, multidrug-resistant *Enterococcus faecium* and methicillin-resistant *Staphylococcus aureus*, fast bacterial killing, insusceptibility to antimicrobial resistance, and high *in vivo* efficiency in infection models. Mechanistic investigations revealed that **1** disrupts the bacterial cell membrane through a mechanism involving interactions between the vancosamine moieties and membrane-embedded phosphatidylglycerol/phosphatidylethanolamine. The results provide insights into the biological generation of vancosamine in natural products and demonstrate the potential of **1** as an effective lead to address the growing antimicrobial resistance threats.

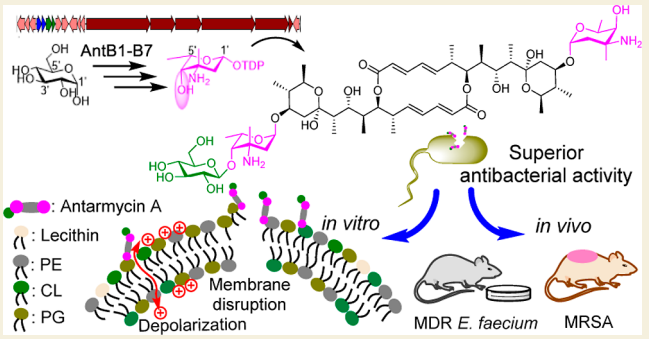

KEYWORDS: *antimicrobial resistance, macrolide, vancosamine, glycosyltransferase*

INTRODUCTION

Antimicrobial resistance (AMR) has emerged as one of the leading global health threats of modern times.[1−4] To guide and promote research and development of new antibiotics, the World Health Organization (WHO) has created a priority list of antibiotic-resistant bacteria for which new antimicrobial development is urgently needed; vancomycin-resistant *Enterococcus faecium* (VRE) and methicillin-resistant *Staphylococcus aureus* (MRSA) are designated as the highest ranked Gram-positive bacteria.[5,6] *E. faecium* is a prominent cause of severe hospital-associated infections, and its inherent resistance to many antibiotics as well as its ability to acquire additional antibiotic-resistant genes make these infections very difficult to treat.[7−10] For instance, hospital-adapted *E. faecium* is now increasingly resistant to vancomycin.[11,12] As a result, there is now effectively no readily viable treatment for many hospital-acquired infections caused by *E. faecium*.[13,14] *S. aureus*, which can cause moderately severe skin and soft tissue infections as well as fatal pneumonia and sepsis, is one of the most notorious and widespread pathogens.[15−18] The widespread distribution of MRSA has resulted in increases in mortality, morbidity, and hospital stays attributable to *S. aureus* infections. In the United States in 2017, the mortality caused by MRSA remained the highest of any antibiotic-resistant pathogen with a death count of 20,000.[19,20] Any viable solution to the AMR crisis clearly relies on the discovery of effective new antibiotics.[21−24]

Natural products (NPs) from microorganisms have played, and continue to play fundamental roles in antibiotic development campaigns, in large part, because of their highly evolved nature.[25−28] More recently, new strategies have dramatically improved the means of uncovering new microbial NP candidates with which to address the increasing AMR crisis.

Received: October 1, 2024
Revised: December 7, 2024
Accepted: December 9, 2024
Published: December 18, 2024

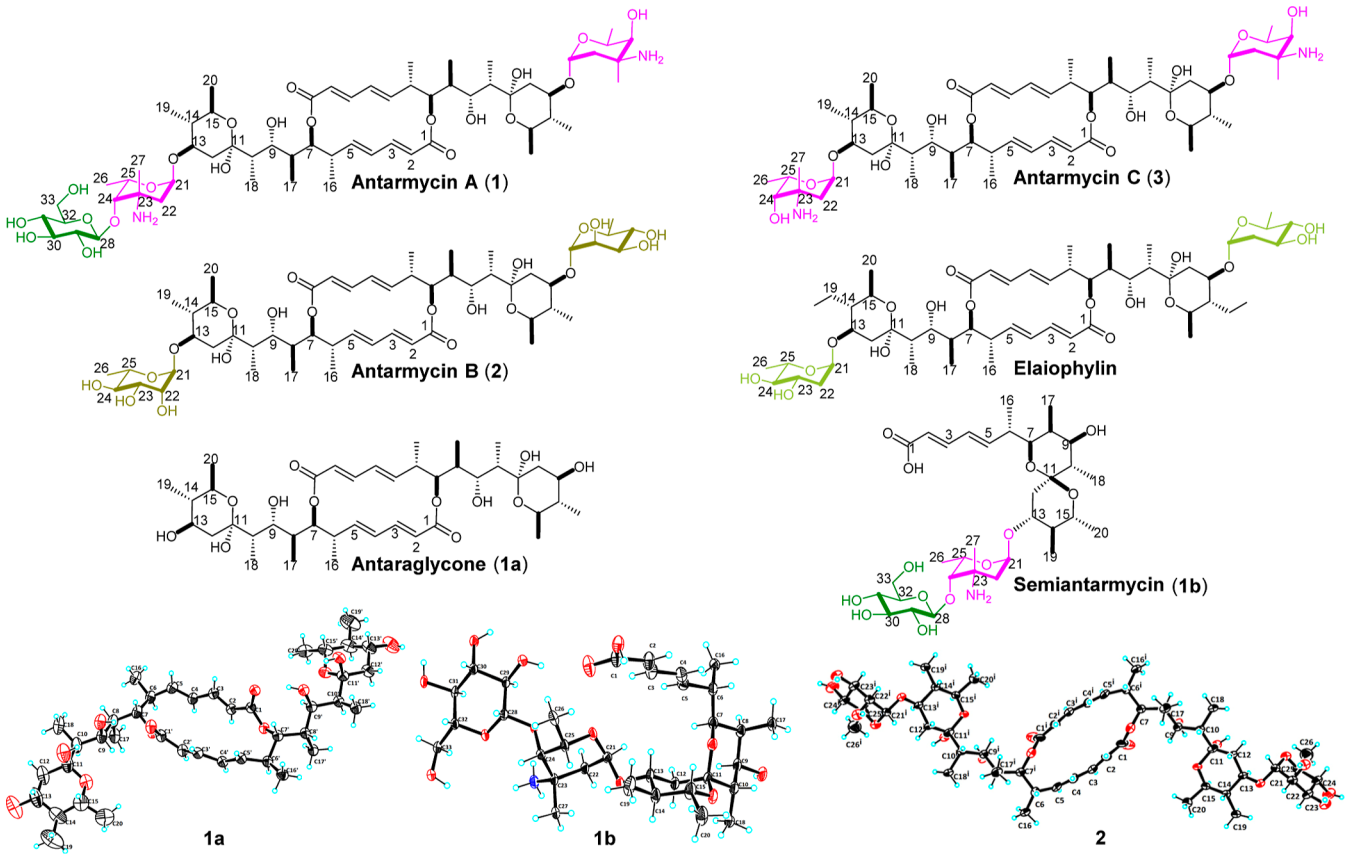

Figure 1. Structures of **1**−**3**, **1a**, **1b**, and elaiophylin as well as single-crystal X-ray structures for compounds **1a**, **1b**, and **2**.

The exploration of new antibiotic-producing strains in underexplored environments, rational activation of plasmid-borne biosynthetic gene clusters (BGCs) represent some of these new strategies.[29−35] Microbes in deep-sea environments, where the transfer of resistance genes from terrestrial organisms is limited, are excellent repositories for new antibiotics with activity against terrestrial AMR.[31,32] In addition, plasmid-borne BGCs, which might be exchanged horizontally via plasmid transfer processes, may encode bioactive molecules that bacteria may employ to gain advantage over other competing microbes in their ecological niches; such systems also have emerged as attractive tools in the search for new bioactive NPs.[33−35]

We report here our discovery of a new antibiotic, antarmycin A (**1**), which displays potent *in vitro* antibacterial activities against a panel of important human pathogens including multidrug-resistant (MDR) *E. faecium* and MRSA, from a deep-sea-derived rare actinomycete *Pseudonocardia antarctica* SCSIO 07407. Antarmycin A (**1**) is a glycosylated macrodiolide found to be encoded within the plasmid pAn001 that features a number of readily transferrable elements. In-depth investigations of the biosynthetic machinery underlying the pendant sugars of **1** enable us to identify the biosynthetic genes responsible for the production of the vancosamine moiety and isolate rhamnose-modified antarmycin B (**2**) and deglucosylated antarmycin C (**3**). Systematic *in vitro* antibacterial assays of the antarmycin series unveiled a structure−activity relationship (SAR) in which the pendant vancosamines appear to dictate potent antimicrobial activities. Further mechanistic investigations revealed that **1** disrupts the bacterial cell membrane through a mechanism involving interactions between vancosamines and phosphatidylglycerol/phosphatidylethanolamine. Moreover, the potent *in vitro* activities of **1** against MDR *E. faecium* and MRSA very efficiently translated into both intestinal and epicutaneous infection models, highlighting the potential of this agent as a new lead in the battle against AMR and its clinical ramifications.

RESULTS AND DISCUSSION

Discovery of Antarmycins from Deep-Sea-Derived *P. antarctica*

The fermentation extract of a rare actinomycete, *P. antarctica* SCSIO 07407 from a sediment sample at a depth of 3386 m was found to effectively inhibit both VRE and MRSA when the fermentation medium was supplemented with 2% macroporous resins to effectively enrich secondary metabolites. Subsequent bioassay-guided chemical investigations of a 30 L culture of this strain led to the isolation of a novel bioactive compound, antarmycin A (**1**). In addition, two other inactive but previously unknown compounds, the macrodiolide skeleton unit-containing antaraglycone (**1a**) and the 6,6-spiroketal polyketide semiantarmycin (**1b**), were isolated at the same time.

Antarmycin A (**1**) was isolated as the major metabolite from the resin-adsorbed extract. (+)-high-resolution electrospray ionization mass spectrometry analysis of **1** retuned a protonated ion indicative of a molecular formula $C_{60}H_{100}N_2O_{21}$, requiring 12 degrees of unsaturation. Detailed analysis of the 1D and 2D NMR data (Table S1 and Figures S31−S37) revealed that **1** possesses a 16-membered symmetric macrodiolide scaffold featuring C_2-symmetry and hemiketal moieties. This scaffold closely resembles the skeleton of

https://doi.org/10.1021/jacsau.4c00912
JACS Au 2025, 5, 237−249

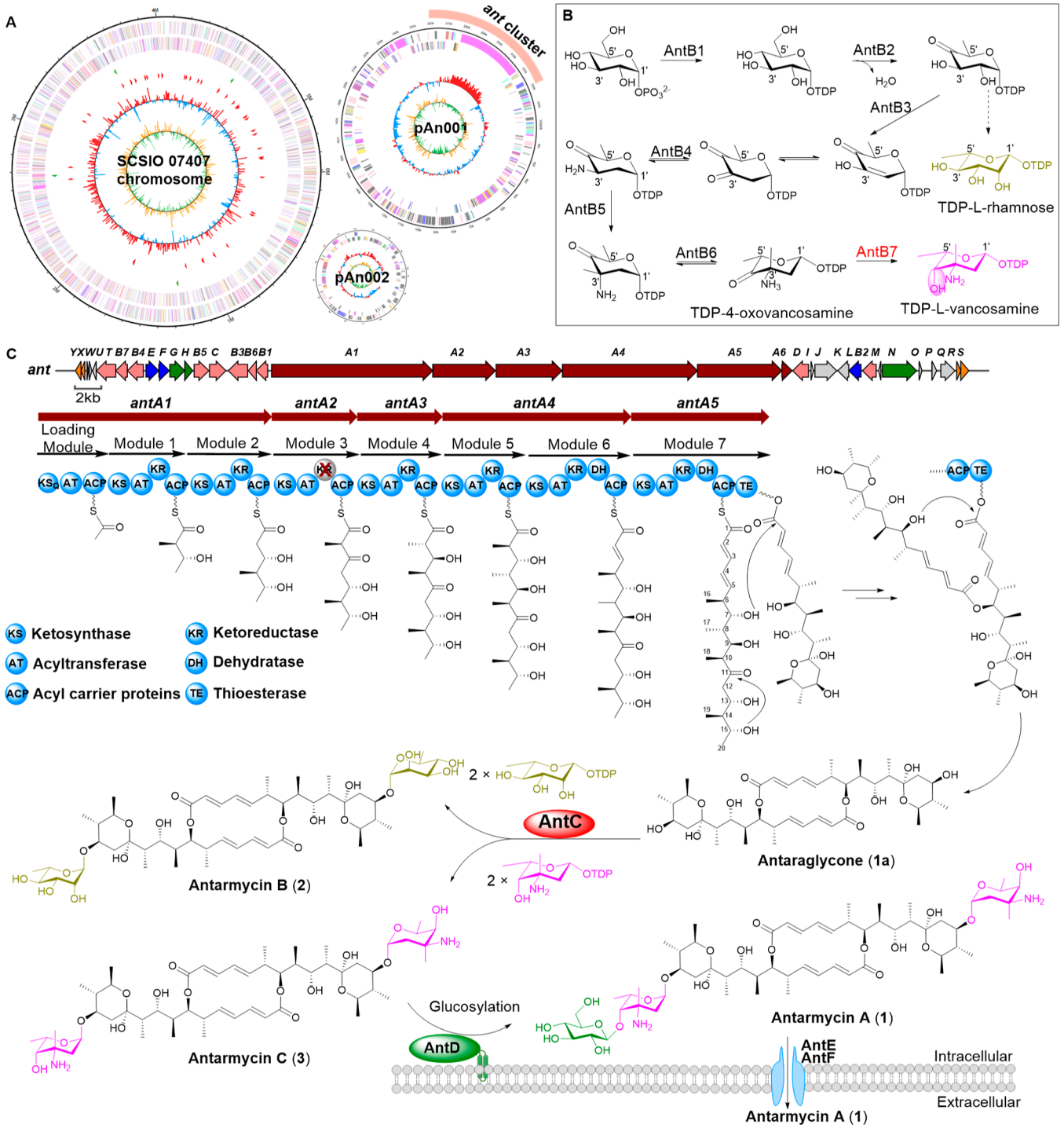

Figure 2. Biosynthesis of antarmycin. (A) Chromosome and plasmids pAn001, pAn002 of *P. antarctica* SCSIO 07407. (B) Proposed biosynthetic pathway of L-vancosamine. (C) Biosynthetic gene cluster and proposed biosynthetic pathway of antarmycins.

elaiophylin,[36] differing only by the presence of a methyl group instead of an ethyl group at C-14 and C-14′ positions (Figure 1). Additionally, 1D NMR data of **1** revealed resonances corresponding to three hexoses, which were further established as two vancosamines and one glucose by correlated spectroscopy (COSY) and heteronuclear multiple bond correlation (HMBC) NMR analyses. Each vancosamine was determined to form a glycosidic bond with the 13-hydroxyl group of each octaketide monomer within the macrodiolide scaffold, as evidenced by the diagnostic HMBC correlation from the hemiketal proton H-21 to C-13 (Figures S1 and S36). The glucose moiety was attached to one of the vancosamine moieties via an ether bond formed between C-24 and C-28 (Figures 1 and S1). Single-crystal X-ray diffraction analysis of the biosynthetic intermediates **1a** and **1b** (Figure 1) isolated from the resin-adsorbed extract allowed us to determine the stereochemistry of the macrodiolide skeleton (6*S*, 7*S*, 8*S*, 9*R*, 10*S*, 11*R*, 13*R*, 14*S*, and 15*R*) and the sugar moieties (two α-L-vancosamines and one β-D-glucose) in the structure of **1**, based on their biosynthetic relationships. Elaiophylins belong to a

https://doi.org/10.1021/jacsau.4c00912
JACS Au 2025, 5, 237−249

family of 16-membered glycosylated macrodiolides featuring unusual C_2-symmetry and a hemiketal moiety. The elaiophylin family shows high structural similarity in the macrodiolide backbone, with major differences in the substituents at C-2 and/or C-2′, C-11 and/or C-11′, as well as C-14 and/or C-14′. With respect to the pendant sugar, except for the 2-deoxyfructose, no other sugars have been reported for this class of natural products.[37] Although **1** shares a macrodiolide scaffold similar to that of elaiophylin, the presence of the deoxyaminosugar vancosamine is unprecedented in this class of macrodiolide natural products.

ANTARMYCINS ARE PRODUCED BY A BGC ENCODED ON A GIANT SELF-REPLICATED PLASMID IN *P. ANTARCTICA* SCSIO 07407

To gain insight into the biosynthetic machinery of antarmycin A (**1**), we sequenced the whole genome of *P. antarctica* SCSIO 07407. The genome of SCSIO 07407 was found to consist of a 5.41 Mbp circular chromosome and two circular plasmids, pAn001 and pAn002 (Figure 2A). BLAST search revealed that the 16S rRNA gene of strain SCSIO 07407 showed the highest similarity (99%) to that of *P. antarctica* DSM 4479^T. Phylogenomic analysis revealed that, at the whole genome level, strain SCSIO 07407 showed an average nucleotide identity (ANI) value of 97% to *P. antarctica* DSM 4479^T, suggesting that SCSIO 07407 and DSM 4479^T should belong to the same species.[38] The major difference between these two genomes is that there are two giant plasmids with sizes >50 kb[39,40] in SCSIO 07407 [pAn001 (352.7 kb) and pAn002 (164.4 kb)], whereas DSM 4479^T was found to contain only one giant plasmid (253.3 kb). The sequencing coverage depth per base on pAn001 and pAn002 was 1.88-fold and 1.86-fold that of the chromosome, respectively, indicating that each plasmid might have two copies in one cell. Plasmid pAn001 is especially distinctive in two ways. First, pAn001 was found to encode a large type I polyketide synthase (PKS) BGC (termed herein *ant*, GenBank accession number OQ475001), containing five consecutive PKS genes (*antA1*−*antA5*) encoding a total of eight modules. Second, pAn001 was found to contain multiple transferrable elements including 29 open reading frames (ORFs) encoding putative transposases and 3 ORFs encoding putative integrases (Table S4), indicating its ability to transfer parts of its sequence, such as the *ant* cluster horizontally, into foreign bacteria.

Given that the symmetric macrodiolide core of antarmycin is composed of two octaketides, the *ant* cluster is most likely responsible for the antarmycin biosynthesis. Inactivation of the KS_Q domain in AntA using established λ-RED-mediated PCR-targeting mutagenesis methods[41] completely abolished the production of compounds **1** and **1a**, demonstrating the indispensability of the *ant* cluster for antarmycin biosynthesis (Figure S5A, trace (ii)). Further bioinformatic analyses of the domains of PKSs AntA1−AntA5 (Table S6) enabled us to propose a plausible biosynthetic pathway for the symmetric macrodiolide core of **1** (Figure 2C). PKSs AntA1−AntA5 are proposed to catalyze two rounds of polyketide synthesis to generate two separate octaketide chains. The biosynthesis of the monomer of the diolide backbone is proposed to start with malonyl-CoA as the starting unit, which is decarboxylated by the KS_Q domain on the loading module. Subsequent chain elongation involves condensations of the starter unit with three malonyl-CoA (modules 2, 6, and 7) and four methylmalonyl-CoA (modules 1, 3, 4, and 5) extender units (Tables S6 and S8, and Figure S4); optionally modified ketoreductase (KR), dehydratase (DH), and enoylreductase (ER) domains in every extender module establish the oxidation state of the β-oxo functionality to afford the full length of monomer octaketide chain. Following the formation of a hemiketal at C-11, we envision that the C-7 hydroxyl group of the monomer octaketide chain (ACP-tethered) of module 7 attacks another monomer bound to the thioesterase (TE) domain to form the C_2-symmetric diolide backbone of **1**. Additionally, the hemiketal at C-11 is likely to be attacked by the transient C-7 hydroxyl group to form the 6,6-spiroacetal of **1b** spontaneously[42,43] (Figure S6). Besides the PKS genes *antA1*−*antA5*, the *ant* cluster also contains genes associated with sugar biosynthesis, regulation, transport, and toxin-antitoxin system (Figure 2C and Table S6). *antE* and *antF*, located upstream of the core PKS genes, encode a putative ATP-binding cassette (ABC) transporter system that can export endogenously produced secondary metabolites and thus prevent self-poisoning in prokaryotes;[44,45] inactivation of *antF* completely eliminated the production of compounds **1** and **1a** (Figure S5B, trace (x)), suggesting that AntE/F might be responsible for exporting the toxic antarmycins.

AntC Transfers Two Vancosamine Moieties to Antaraglycone (1a), Whereas AntD Tethers One Glucose to Only One of the Vancosamines

We next explored the biosynthetic machinery responsible for sugar installation. We first focused on the biosynthesis and transfer of L-vancosamine attached to each monomer of the symmetric diolide. Vancosamine is a terminal deoxysugar attached to the aglycone of the glycopeptide antibiotic, vancomycin; this deoxysugar has been shown to be crucial for antimicrobial potency by affecting back-to-back dimerization constants for the antibiotic molecule.[46] The biosynthetic pathway for vancosamine in vancomycin has not yet been elucidated by biological experiments. However, the biosynthesis of 4′-epi-vancosamine in chloroeremomycin, another member of the vancomycin family of antibiotics, has been demonstrated to involve the inversion of TDP-4′-keto-6′-deoxyglucose, via TDP-L-4′-oxovancosamine, to TDP-L-4′-epivancosamine by a set of five enzymes, EvaA−EvaE. This process involves C-2′ deoxygenation, C-3′ amination and methylation, C-5′ epimerization, and C-4′ ketoreduction.[47] Given the structural similarities between vancosamine and 4′-epi-vancosamine, we speculated that the biosynthesis of vancosamine in the antarmycin-producing strain might also involve a set of four enzymes homologous to EvaA−EvaD catalyzing the inversion of TDP-4′-keto-6′-deoxyglucose to TDP-L-4′-oxovancosamine, but an enzyme distinct from the C-4′ ketoreductase EvaE[47] would likely need to be dedicated to the C-4′-ketoreduction of TDP-L-4′-oxovancosamine to generate TDP-L-vancosamine.

Inspection of the *ant* cluster revealed that there is indeed a set of four genes *antB3*−*antB6* encoding enzymes homologous to EvaA−EvaD responsible for the production of TDP-L-4′-oxovancosamine from TDP-4′-keto-6′-deoxyglucose. In contrast to the chloroeremomycin BGC, the *ant* cluster contains two genes *antB1* and *antB2* encoding the putative glucose-1-phosphate thymidylyltransferase and dTDP-glucose 4,6-dehydratase involved in the conversion of glucose-1-phosphate to TDP-4′-keto-6′-deoxyglucose (Table S6). Inspired by this realization, *antB1*−*antB6* were speculated to catalyze the transformation of glucose-1-phosphate to TDP-L-4′-oxovan-

https://doi.org/10.1021/jacsau.4c00912
JACS Au 2025, 5, 237−249

cosamine as shown in Figure 2B. Inactivation of *antB1*, *antB3*, *antB4*, *antB5*, and *antB6* completely abolished the production of **1** but still permitted antaraglycone (**1a**) assembly, clearly implicating them in vancosamine biosynthesis (Figure S5B). Inactivation of *antB2* appeared to have no significant influence on the production of **1** and **1a** (Figure S5B), which can likely be attributed to the compensatory actions of the other putative TDP-glucose 4,6-dehydratase, ORF_908 (similarity/identity: 64%/49%), encoded in the chromosome. Consistent with the opposite stereochemistry of the C-4′ hydroxyl group, the *ant* cluster did not encode a homologue corresponding to the C-4′ ketoreductase, EvaE, from the SDR family in the 4′-epivancosamine biosynthetic pathway. Alternatively, *antB7*, encoding an F420-dependent oxidoreductase, was speculated to catalyze the reduction of a transient 4′-ketone thus yielding the axial hydroxyl group of the vancosamine moiety. Inactivation of *antB7* led to the complete abolishment of antarmycin A (**1**) production and accumulation of aglycone **1a** (Figure S5B). The production of **1** was restored by *trans* complementation of *antB7* (Figure S5C), validating its involvement in vancosamine biosynthesis. Importantly, once vancosamine is available, it must be added to the macrocyclic diolides to confer antimicrobial activity. Bioinformatic analyses revealed that there are two glycosyltransferases, AntC and AntD, encoded in the *ant* cluster. AntC shows similarity to GtfD (similarity/identity: 51%/39%), the glycosyltransferase that carries out vancosamine transfer in the vancomycin pathway,[48,49] suggesting that AntC might carry out similar chemistry during the assembly of **1**. Indeed, inactivation of *antC* produced a mutant strain unable to generate intact **1**; rather, the Δ*antC* mutant accumulated antaraglycone (**1a**) devoid of vancosamine (Figure S5A, trace (iii)). These results demonstrated that AntC catalyzes the transfer of one vancosamine to each monomer of symmetric antaraglycone (**1a**). In addition, we noted that all *antB1*−*antB7* mutant strains accumulated a new intermediate (**2**, termed antarmycin B) with a retention time distinct from those of **1** and **1a** (Figure S5B). Compound **2** was subsequently isolated from the Δ*antB3* mutant strain due to the high rate of production of this intermediate by this mutant strain. Comprehensive HRMS, NMR, and X-ray diffraction data analyses are available (Table S1 and Figures S29 and S52−S58) revealed that **2** derives from **1** but with an α-L-rhamnose attached to each octaketide monomer of the symmetric macrodiolide at C-13 (Figure 1). The isolation of **2** from mutant strains resulting from vancosamine biosynthetic gene inactivation indicated that the glycosyltransferase AntC exhibits at least moderate substrate promiscuity with respect to glycosyl donors.

Following vancosamine linkage to **1a**, one of the pendant vancosamine moieties must be glucosylated to afford antarmycin A (**1**). AntD, the other uncharacterized glycosyltransferase encoded in the *ant* cluster, is an excellent glycoyltransferase candidate. Inactivation of *antD* completely abolished the production of **1**, which was restored via *in trans* complementation of *antD* (Figure S5A, trace (iv); S5C, trace (iv)). In addition, the Δ*antD* mutant strain accumulated a new intermediate (**3**). Consequently, we fermented the Δ*antD* mutant strain on a large scale to obtain quantities of **3** sufficient for structural elucidation. HRMS and intensive NMR analyses (Table S1 and Figures S29 and S59−S65) revealed that **3** (termed antarmycin C) is a derivative of **1** devoid of the vancosamine−glucose linkage, strongly supporting the proposed role of AntD in glucosylation. To validate its *in vitro* biochemical activity, we first tried to overexpress and purify AntD from *Enterococcus coli* BL21 (DE3). Unfortunately, most AntD proteins were overexpressed as insoluble inclusion bodies (Figure S7). Further bioinformatic analysis revealed that AntD was predicted to be a membrane-associated enzyme (Figure S8), explaining, in part, the observed insolubility. As an alternative approach, we prepared a lipid microsomal fraction of the recombinant *E. coli* BL21 (DE3) expressing AntD. Using this prepared lipid microsomal fraction containing AntD as a catalyst, complete conversion of **3** to **1** in the presence of UDP-D-glucose was readily observed (Figure 3, trace (ii)),

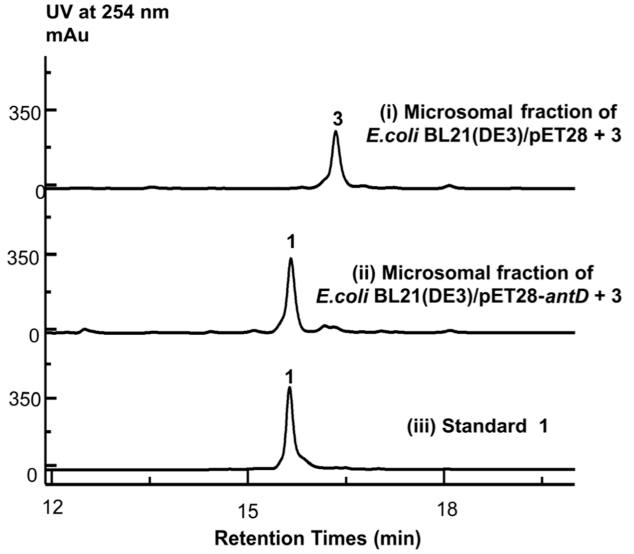

Figure 3. *In vitro* microsomal fraction assays of AntD: (i) control assay with **3** and the lipid microsomal fraction of *E. coli* BL21(DE3) containing the empty expression plasmid pET28a; (ii) reaction using **3** and lipid microsomal fraction of *E. coli* BL21(DE3) containing the AntD expression plasmid pET28a-*antD*; (iii) authentic standard of **1**.

whereas the lipid microsomal fraction prepared from the *E. coli* BL21 (DE3) harboring the empty vector control failed to yield any detectable amounts of **1** (Figure 3, trace (i)). Collectively, the *in vivo* gene inactivation and *in vitro* biochemical experiments validated the notion that AntD is indeed responsible for vancosamine glucosylation *en route* to compound **1**.

Antarmycin A Shows Potent *In Vitro* Antimicrobial Activity against Important Drug-Resistant Pathogens

To begin to establish structure−activity relationships (SARs) for the antarmycins, analytically pure **1**−**3**, **1a**, and **1b** were systematically assessed for possible antimicrobial activities (Tables 1 and S3). Antarmycin A (**1**) was found to be exceptionally active against nine clinically relevant multidrug-resistant (MDR) isolates of *E. faecium*, which are highly resistant to at least eight of ten clinically used antibiotics including vancomycin (Table S2), with MIC values spanning 0.25−0.5 μg/mL. Compound **1** also was active against 13 clinical isolates of MRSA, with MIC values spanning 1−4 μg/mL. In a time-dependent killing curve analysis, **1** showed rapid bactericidal activity against MRSA and MDR *E. faecium*, with more than 3 orders of magnitude reduction in colony-forming units (CFUs) observed within 4 h at 2−8-fold MIC (Figure S9). Significantly, the antibacterial activities of **1** extended to seven other Gram-positive pathogens including *Enterococcus*

https://doi.org/10.1021/jacsau.4c00912
JACS Au 2025, 5, 237−249

Table 1. MIC Values of Antarmycins A−C (1−3)

strains	MIC values ($\mu g\ mL^{-1}$)			
drug-resistant G^+ pathogens	**1**	**2**	**3**	vancomycin
E. faecium 35682 (MDR)	0.5	32	0.25	>128
E. faecium 36711 (MDR)	0.5	16	0.125	>128
E. faecium 36235 (MDR)	0.5	32	0.25	128
E. faecium 36950 (MDR)	0.5	16	0.5	16
E. faecium 0847 (MDR)	1	16	0.5	16
E. faecium 4174 (MDR)	0.5	16	0.125	16
E. faecium 08257 (MDR)	0.5	16	0.25	>128
E. faecium 08369 (MDR)	1	16	0.25	64
E. faecium 0661 (MDR)	0.5	16	0.125	>128
MRSA 16162	4	64	1	1
MRSA 718306	2	32	1	2
MRSA 16339	2	32	1	1
MRSA 6917	4	16	1	1
MRSA Shhs-E1	4	64	1	2
MRSA 745524	2	32	0.5	2
MRSA 1862	2	32	1	0.5
MRSA 991	4	32	1	1
MRSA 669	4	16	0.5	0.5
MRSA 001	2	16	0.5	4
MRSA GDQ6P012P	1	16	0.5	0.5
MRSA 3090	2	32	1	0.5
MRSA USA300	2		0.25	1
other G^+ pathogens	**1**	**2**	**3**	vancomycin
E. faecalis ATCC 29212[a]	0.25	32	0.25	2
E. gallinarum 5F52C[a]	1		0.25	4
S. hemolyticus[a]	2		0.25	2
S. epidermidis[a]	1		0.25	1
S. pneumoniae ATCC 49619[a]	8		2	2
B. subtilis 168[a]	1		0.5	0.25
B. cereus[a]	2		0.5	2
G^- pathogens	**1**	**2**	**3**	metronidazole
H. pylori HpG27[a]	2		0.5	2
H. pylori HpG129	4		1	16
P. aeruginosa ATCC 27853	32	>128	64	
A. baumannii 15122	>128	>128	>128	
E. coli 920	>128	>128	>128	
K. pneumoniae 14578	>128	>128	>128	
fungal strains	**1**	**2**	**3**	fluconazole
C. albicans SC5314[a]	16		8	0.5
C. albicans C5	8		4	>64
C. neoformans ATCC 4906[a]	16		8	4

[a]Common laboratory strain.

faecalis, *Enterococcus gallinarum*, *Staphylococcus hemolyticus*, *Staphylococcus epidemirdis*, *Staphylococcus pneumoniae*, *Bacillus subtilis*, and *Bacillus cereus*. Compound **1** was inactive against most Gram-negative bacteria assayed (Tables 1 and S3), but it showed good activity against two strains of *Helicobacter pylori*, the organism believed to drive gastritis and gastric cancer.[50−52] In addition, **1** was found to possess antifungal activity against *Candida albicans* and *Cryptococcus neoformans*. Specifically, **1** inhibited the growth of the drug-resistant clinical isolate *C. albicans* C5 with an MIC of 8 μg/mL, far superior to the clinically important antifungal drugs fluconazole (Table 1). Another noteworthy observation is that **3**, which is devoid of the glucose moiety seen in **1**, was generally 2−8-fold more potent than **1** against almost all Gram-positive pathogens tested (Table 1). Bioassays with compound **2**, possessing two rhamnose moieties instead of the vancosamine moieties displayed by **3**, revealed significantly lower activities against Gram-positive bacteria with MIC values spanning 32−64 μg/mL. In contrast to **1**, **2**, and **3**, both the aglycone **1a** and the 6,6-spiroketal polyketide **1b** were inactive (MIC >64 μg/mL) against all pathogens evaluated (Table S3). These results suggest an important role for glycosylation in imparting antibacterial activities for the antarmycin series of compounds. Specifically, the deoxysugar vancosamine linked at C-13 of the macrodiolide is vital to antibacterial potency, whereas decoration of one of the vancosamine moieties with a glucose moiety attenuates the potency. To further delineate the importance of the deoxysugar for antibacterial potency, elaiophylin,[36] which contains a macrodiolide core decorated with two 2′-deoxyfucose moieties (Figure 1), was isolated from the previously reported *Streptomyces sp.* SCSIO ZS0520[53] and subjected to antibacterial assays. The results of bioassays showed that elaiophylin was as active as compound **3** but generally 2−4-fold more potent than compound **1** against MDR *E. faecium* and MRSA (Table S3), indicating the SAR notion that deoxygenation at C-2′ of the sugars linked at C-13 of the macrodiolide, such as vancosamine in compounds **1** and **3** and 2′-deoxyfucose in elaiophylin, is vital to the antibacterial activity of this class of macrodiolide natural products. Although compound **3** and elaiophylin show more potent antibacterial activities than compound **1**, **1** was superior to **3** and elaiophylin as reflected by its HC_{50} value of 3 μg/mL, IC_{50} values spanning 2.0−3.0 μg/mL against three normal cell lines, and the resulting relatively high antibacterial selectivity index (HC_{50}/MIC = 6, IC_{50}/MIC = 4−6) (Table S16). Overall, the results of these *in vitro* assays suggested that, of the agents identified here, compound **1** holds the greatest promise for antibacterial drug development initiatives.

Antarmycin A (1) Shows High *In Vivo* Efficacy against MDR *E. faecium* and MRSA

Given the potent *in vitro* activities of **1** against MDR *E. faecium* and MRSA, we next explored its potential as a therapeutic agent to treat infections caused by these pathogens. *E. faecium* is one of the most infamous examples of an intestinal colonizer, which can cause severe systemic infection after translocation from the intestinal tract into the bloodstream. Reducing *E. faecium* abundance within the intestine and thereby preventing its translocation to blood has been as an effective strategy to treat *E. faecium*. To test the *in vivo* efficacy of **1** against MDR *E. faecium*, we used an intestinal infection model with MDR clinical isolate 36235 of *E. faecium* as the challenge pathogen; this strain was isolated from a patient subjected to multiple courses of antibiotics during prolonged hospitalization and exhibited high resistance to 10 clinically used antibiotics (Table S2). Immuno-compromised mice were intragastrically infected with MDR clinical isolate 36235 of *E. faecium*. After 24 h of infection, compound **1** was delivered intragastrically at a dose of 60 mg/kg once a day for 3 days; this dose was set based on the dose of the positive drug gentamicin. Compound **1** was shown to be highly efficacious in these MDR *E. faecium* infected mice; a significant reduction in CFUs to a level below

https://doi.org/10.1021/jacsau.4c00912
JACS Au 2025, 5, 237−249

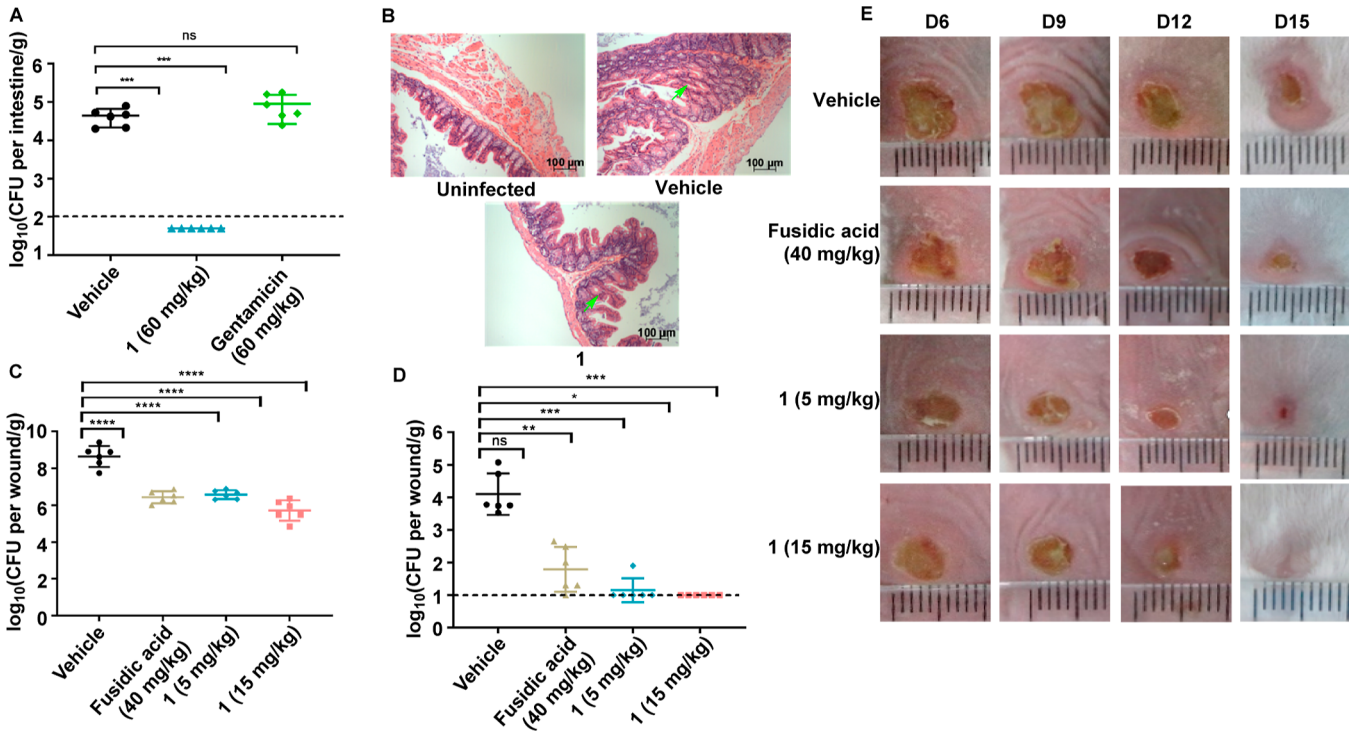

Figure 4. *In vivo* efficacy of antarmycin A. (A) CFUs of *E. faecium* measured from gastrointestinal tissue samples in the intestinal infection model. The baseline of $\log_{10} = 2$ represents the lower limit of detection. (B) Histopathological analysis of the large intestine by hematoxylin and eosin (H&E) staining. Green arrows, villi. (C) CFUs of MRSA measured from the infected sites at 6 d postinfection in the epicutaneous infection model. (D) CFUs of MRSA measured from the infected sites at 15 d postinfection in the epicutaneous infection model. The baseline of $\log_{10} = 1$ represents the lower limit of detection. (E) Mound area at the infected sites in the epicutaneous infection model. The CFUs from each mouse are plotted as individual points, and error bars represent the deviation within an experiment group. For each group, $n = 6$ mice.

the limit of detection was clearly noted in the large intestines of the subjects (Figure 4A). In addition, histopathological examinations of the intestinal tissues showed severe structural compromise with infiltration of immune cells and a lack of villi in mice treated with the vehicle; however, no obvious infiltration of immune cells was observed in mice treated with **1** (Figure 4B), indicating that compound **1** efficiently cleared *E. faecium* from the intestine. Moreover, compared with the mice treated with the vehicle, no notable changes of body weight were observed in the mice treated with **1** (Figure S10), indicating the low toxicity of **1** when administrated intragastrically to treat the intestinal infection caused by MDR *E. faecium*. This low *in vivo* toxicity might be attributed to the intestinal absorption and liver detoxification of **1** when administrated intragastrically.

As MRSA is the most common cause of severe skin and soft tissue infections, we next employed a mouse epicutaneous infection model to assess the activity of **1** against MRSA. Mice were infected intradermally with the clinical strain MRSA USA300. At 3 days postinfection, **1** was administered intradermally at the infection sites at doses of 5 and 15 mg/kg per day given twice a day for 3 days. At 6 days postinfection, **1** was found to cause a 2 $\log_{10}$ reduction of CFUs at the infected sites, with reductions at the lower dose (5 mg/kg) equivalent to that of fusidic acid at 40 mg/kg (Figure 4C). At 15 days postinfection, the CFUs isolated from the infection sites treated with compound **1** were further decreased to a value reaching the limit of detection (4 $\log_{10}$ reduction of CFUs) (Figure 4D). In addition, compound **1** also can significantly reduce the wound area at the infection sites, with the wound nearly completely healed at 15 mg/kg after 14 d infection (Figures 4E and S11). As in the intestinal model, mice in the epicutaneous infection model appeared to neither lose nor gain any body weight in response to the treatment of **1** (Figure S12). These data demonstrated that compound **1** also showed high efficacy in a mouse model of MRSA epicutaneous infection, showcasing its promise as a topical agent lead against MRSA epicutaneous infections.

Mechanism of Action of Antarmycins against Important Drug-Resistant Pathogens: the Role of Cell Membrane Disruption

Given the potent activities displayed by antarmycins, we next sought to elucidate possible MoAs for these agents. We first attempted to raise resistant mutants of *S. aureus* by direct plating on media with a low dose (4× MIC) of antarmycin A (**1**) or by serial passage in the presence of sub-MIC levels of antarmycin A (**1**) over a period of 24 days. In these resistance development experiments, we never obtained any colonies with increased MICs (Figure S13), indicating that antarmycins might not target a protein. To explore the possibility that antarmycin A exerts its antibacterial activity via cell membrane disruption, we first tested it for membrane depolarization activity using a 3, 3′- dipropylthiadicarboncyanine iodide [$DiSC_3(5)$]-based fluorescence assay. The fluorescence intensity of $DiSC_3(5)$ rapidly increased when *S. aureus* was exposed to **1** (4× MIC) (Figure 5A), suggesting membrane depolarization. Further, the cell lytic activity for **1** was also tested using a SYTOX-based fluorescence assay. An increase in SYTOX fluorescence intensity was immediately detected after the addition of **1** to *S. aureus* (Figure 5B), indicating disruption of the cell membrane and subsequent penetration of SYTOX.

https://doi.org/10.1021/jacsau.4c00912
JACS Au 2025, 5, 237−249

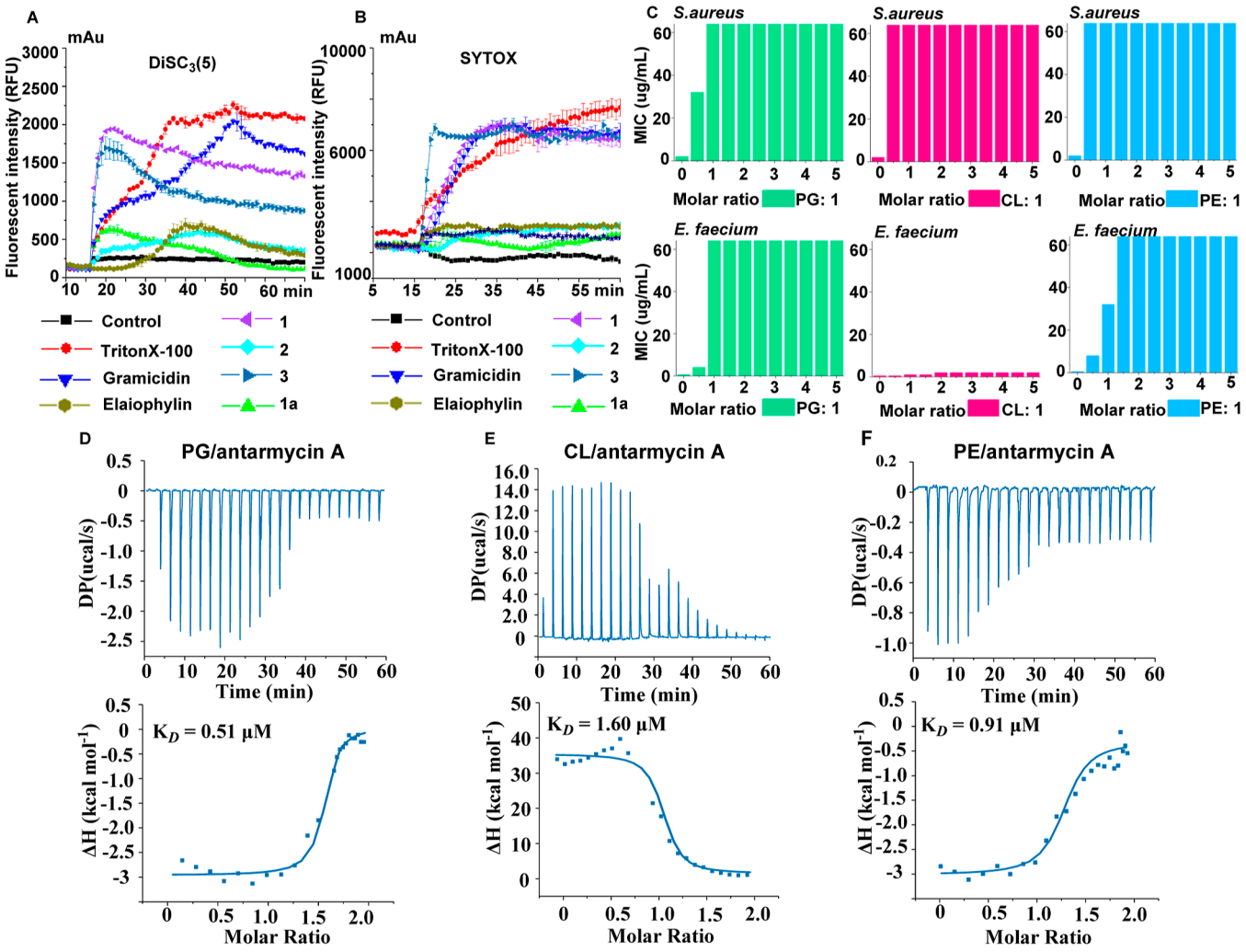

Figure 5. Mode of action of antarmycin. (A) Cell membrane depolarization in **1**−**3**, **1a**, and elaiophylin treated *S. aureus* cultures was monitored using $DiSC_3(5)$. (B) Cell lysis of *S. aureus* cells treated with **1**−**3**, **1a**, and elaiophylin was monitored using SYTOX. (C) MICs of **1** against *S. aureus* and *E. faecium* in the presence of different molar ratios of phosphatidylglycerol, cardiolipin, and phosphatidylethanolamine. (D−F) Isothermal titration calorimetry (ITC) analysis of the interaction of **1** with PG, CL, and PE, respectively.

Collectively, these results indicated that compound **1** targets bacterial cell membranes. It is notable that **1** had no membrane depolarization effect on the Gram-negative *Pseudomonas aeruginosa* ATCC 2785 (Figure S14), consistent with the results of antibacterial assays that **1** was inactive against most Gram-negative bacteria, suggesting that the outer membrane of Gram-negative bacteria blocks these compounds' access to their inner membrane.

To identify cell membrane components specifically targeted or bound by antarmycin, we evaluated the impact of different membrane phospholipids, including phosphatidylglycerol (PG), phosphatidylethanolamine (PE), cardiolipin (CL), lecithin, and distearoyl lecithin, on the antibacterial activity of antarmycin A. The microbroth dilution assay showed that the antibacterial activity of compound **1** against *S. aureus* ATCC 29213 and *E. faecium* 36235 was dose-dependently reduced upon the addition of increasing concentrations of PG and PE, respectively (Figure 5C). These results indicated that antarmycin A may bind to the cell membrane lipids PG and PE, resulting in the disruption of the bacterial cell membrane. It is noteworthy that the antibacterial activity of antarmycin against *E. faecium* remained unaffected even when CL was added at a 10-fold molar excess, whereas the activity of antarmycin A against *S. aureus* was completely abolished with the addition of an equal molar amount of CL (Figure 5C). This differential effect is likely due to the higher affinity of other types of phospholipids in the cell membrane of *E. faecium* 36235 for antarmycin compared to CL or to the lower percentage of CL in the *E. faecium* 36235 cell membrane.

To further identify the important structural elements of antarmycins that interact with PG/PE/CL, compounds **1a**, **2**, and **3** as well as elaiophylin were also subjected to [$DiSC_3(5)$]- and SYTOX-based fluorescence assays. Activity comparisons using data generated with aglycone **1a**, **1**−**3**, and elaiophylin (Figure 5A,B) clearly indicated that the sugar moieties of these compounds are important for cell membrane associations. By comparing the activities of compounds **1**−**3** and elaiophylin to each other, compound **2** and elaiophylin were found to exert comparable membrane depolarization and cell lytic activities; however, these activities were much lower than those found for compounds **1** and **3** (Figures 5B and S15). These findings show that although elaiophylin exhibits superior *in vitro* antibacterial activity to compound **1**, elaiophylin appears to interact with the membrane unlike **1**, suggesting that

https://doi.org/10.1021/jacsau.4c00912
JACS Au 2025, 5, 237−249

elaiophylin has a mode of action different from antarmycin serial compounds. These findings also suggest that the vancosamine sugars, the most substantial structural difference across these compounds, are the most vital structural component driving antarmycin-membrane associations. Subsequent isothermal titration calorimetry (ITC) assays showed that compounds **1** and **3** bearing two vancosamine moieties exhibited good affinity to PG/CL/PE with dissociation constant (K_D) values in submicromolar and micromolar range for PG/PE and CL, respectively (Figures 5D−F and S16), similar to the previously described membrane-targeting compounds isobavachalcone and neolignan-AMP mimic conjugates.[54,55] These results demonstrated that compound **1** indeed interacts with PG/CL/PE, and the vancosamine sugars are the important structure elements for the interaction of antarmycin with the cell membrane. We posit that vancosamine−membrane interactions may be driven predominantly by attractive charge−charge interactions; the negatively charged phospholipids are more effectively bound by antarmycins displaying the greatest number of positively charged vancosamines.

CONCLUSIONS

Herein, the antimicrobial agent antarmycin A (**1**) and two inactive analogues, antaraglycone (**1a**) and semiantarmycin (**1b**) were discovered from a deep-sea-derived rare actinomycete *P. antarctica* SCSIO 07407. Displaying potent activity against MDR pathogens, antarmycin A (**1**) was determined to be a glycosylated macrolide bearing two pendant vancosamine and one glucose moieties by a combination of HRMS, NMR, and X-ray diffraction analyses. The *ant* BGC encoding for construction of **1** was unexpectedly found on a giant self-replicated plasmid pAnt001 featuring 29 transposase- and 3 integrase-type ORFs, indicating a high degree of transfer potential between bacterial species. This is particularly interesting in the case of *P. antarctica* SCSIO 07407, which lives in a deep-sea environment. We envision that acquisition of the *ant* BGC through plasmid-mediated exchange enabled this strain to better tolerate harsh marine conditions, in part, by endowing SCSIO 07407 with the chemical defenses rendered by **1**. More generally, the discovery of antarmycin A (**1**) highlights plasmid-borne BGCs as attractive targets for the mining of novel biologically active NPs in the future. In-depth investigations of the biosynthetic machinery underlying the pendant sugars revealed that the final C-4′-ketoreduction step in the vancosamine biosynthetic pathway is catalyzed by an F420-dependent oxidoreductase AntB7. AntB7 is distinct from SDR family members such as the C-4′-ketoreductase involved in the biosynthesis of 4′-epi-vancosamine. The assignment of AntB7 in this study provides insights into how this deoxysugar is generated in the vancomycin-producing strain. In addition, the biosynthetic investigations also revealed that two glycosyltransferases, AntC and AntD, carry out critical glycosylations and enabled isolation of a rhamnose-modified antarmycin B (**2**) and a deglucosylated-antarmycin C (**3**) from the genetically engineered mutant strains. Systematic *in vitro* antimicrobial assays of compounds **1**−**3**, **1a**, and **1b** and structural related elaiophylin demonstrated that **1** exhibits potent antimicrobial activities against a panel of important human pathogens including MDR *E. faecium* and MRSA and that deoxygenation at C′-2 of sugar moieties linked at C-13 of the macrodiolide is critical to antimicrobial potency of antarmycin serial compounds. Further mechanism of action studies revealed that antarmycin A (**1**) targets the bacterial cell membrane by establishing specific interactions between its vacosamine moieties and phosphatidylglycerol/phosphatidylethanolamine membrane constituents. Most impressive is that antarmycin A (**1**) proved to be effective *in vivo* against MDR *E. faecium* and MRSA in both intestinal and epicutaneous infection models, demonstrating the potential of **1** as an important lead in efforts to address the growing global health crisis of MDR infectious diseases.

METHODS

Bacterial Strains and Plasmids

Bacterial strains and plasmids used in this work are given in Table S9. *P. antarctica* SCSIO 07407 and its mutant strains were cultured on the modified ISP2 medium (ISP2 medium supplemented with 0.4% yeast extract, 1% malt extract, 0.4% glucose, and 3% sea salt) plates at 28 °C for sporulation. *E. coli* DH5α and *E. coli* BL21(DE3) were used for cloning and protein overexpression, respectively.

Chemical Characterization of Antarmycins

Details regarding the general chemical procedures, as well as fermentation, isolation, and structural elucidation of compounds **1**, **1a**, **1b**, **2**, and **3** can be found in Supporting Information

Construction of Mutant Strains of *P. antarctica* SCSIO 07407

To construct mutant strains of *P. antarctica* SCSIO 07407, we first constructed the genomic cosmid library of *P. antarctica* SCSIO 07407 using SuperCosI according to the manufacturer's protocol provided by the vector kit (Agilent). Approximately 3,200 clones were selected, placed in 96-well plates, and stored at −80 °C. Five pairs of primers (Table S10) were designed and used for library screening. Four overlapping positive cosmids (7#9E, 17#9F, 21#4G, and 2#9E) containing all biosynthetic genes were obtained. We next used the λ-RED-mediated PCR-targeting mutagenesis method for gene inactivation for *P. antarctica* SCSIO 07407.[41] Primers designed for the inactivation of each gene are listed in Table S11. Cosmids 7#9E, 17#9F, 21#4G, and 2#9E were each transformed into *E. coli* BW25113/pIJ790 for gene inactivation. Gene disruption cassette *aac(3)IV-oriT* was amplified using a fragment from plasmid pIJ773 that was digested with *Eco*R I and *Hin*d III. PCR products of the *aac(3)IV-oriT* cassette for each disrupted gene were electroporated into *E. coli* BW25113/pIJ790 containing one of the above cosmids for λ-RED-mediated recombination to yield recombinant cosmids pJuPA001−pJuPA012 (Table S9). These recombinant cosmids were transformed into *E. coli* ET12567/pUZ8002 and then conjugated with the *P. antarctica* SCSIO 07407 wild-type strain. Double crossover mutants were first selected on the basis of the kanamycin^{S}apramycin^R phenotype and then further confirmed by PCR using primers listed in Table S12 (for gel analysis, see Figures S17−S28). Finally, 11 mutant strains of *P. antarctica* SCSIO 07407, Δ*antA1*, Δ*antB1*, Δ*antB2*, Δ*antB3*, Δ*antB4*, Δ*antB5*, Δ*antB6*, Δ*antB7*, Δ*antC*, Δ*antD*, and Δ*antF*, were generated (Table S15).

Complementation of Δ*antB7*, Δ*antC*, and Δ*antD* Mutant Strains

The complementation of Δ*antB7*, Δ*antC*, and Δ*antD* mutant strains followed the same procedure, and an example for complementation of Δ*antB7* mutant strain is detailed here. The coding region of *antB7* was amplified with primers B7-expF/B7-expR (Table S13). The purified PCR products were digested by *Nde* I/*Bam*H I and then cloned into the same cleavage sites of a pSET152-derived integrating expression plasmid, pL646ATE,[56] under the control of a strong constitutive promoter *ermE**p. The recombinant plasmid pL646ATE-*antB7* was then transformed into *E. coli* ET12567/pUZ8002 and transferred into the Δ*antB7* mutant strain by conjugation. The exconjugants resistant to thiostrepton were selected and further confirmed by PCR, generating the complementation strain Δ*antB7*:*antB7*.

https://doi.org/10.1021/jacsau.4c00912
JACS Au 2025, 5, 237−249

Preparation of Microsomal Fraction of AntD

The coding region of *antD* was amplified by PCR using cosmid 7#9E as the template with a pair of primers of pET28a-*antD*-F/R (Table S14). The purified PCR products were digested with *Nde* I and *Eco*R I and cloned into the same restriction sites of the pET28a(+) expression vector. After confirmation by sequencing, recombinant plasmid pET28a-*antD* was transformed into *E. coli* BL21(DE3). The *E. coli* BL21(DE3)/pET28a-*antD* was cultured at 28 °C and 200 rpm to OD_{600} = 0.6. Isopropyl *β*-*D*-1-thiogalactopyranoside (IPTG) was then added to a final concentration of 0.1 mM to induce the expression of AntD. After cultivation at 16 °C for an additional 18 h, the cells were collected by centrifugation, washed with 50 mM Tris−HCl buffer (pH 8.0) twice and resuspended in Buffer A (0.6 M sorbitol, 0.1 M KCl, 1.0 mM ethylenediaminetetraacetic acid (EDTA), 1.0 mM dithiothreitol (DTT), 1.0 mM DMSF, 50 mM Tris−HCl, pH 7.5). The cell suspension was then sonicated on ice to obtain a homogenate. The homogenate was centrifuged (14,000 rpm at 4 °C for 10 min), and the supernatant was further fractionated by ultracentrifugation at 100,000*g* and at 4 °C for 6 h. The microsome extracts were then resuspended in 500 μL of Buffer B (20% glycerol, 1.0 mM EDTA, 1.0 mM DTT, 50 mM Tris−HCl, pH 7.5) and stored at −80 °C.

In Vitro Biochemical Activities of Microsomal Fraction of AntD

Assay for AntD microsome bioactivity was performed with 0.2 mM UDP-*α*-D-glucose, 10 mM $MgCl_2$, and 2 μM substrate **3** in 100 μL of the prepared microsomal fraction of AntD at 30 °C for 8 h. The reaction was quenched by the addition of 100 μL of MeOH. After the removal of solvent in vacuo, the extract was dissolved in MeOH for HPLC analysis. The microsomal fraction from *E. coli* BL21(DE3) was used as a negative control.

Antibacterial Activities and Cytotoxicity Assay

The antibacterial activities of compounds **1**−**3**, **1a**, **1b**, and elaiophylin were assessed using 2-fold serial dilutions of antibacterial agents in MH broth, according to previously reported standard methods provided by Clinical and Laboratory Standards Institute (CLSI).[57] The cytotoxicity of compounds **1**−**3**, **1a**, **1b**, and elaiophylin were evaluated using Cell Counting Kit-8 according to the manufacturer's instructions (CCK-8, DojinDo).

In Vitro Hemolysis Assay

Fresh whole rabbit blood was drawn from a healthy rabbit and defibrinated. The whole blood cells were then washed with PBS three times and diluted with PBS to a final concentration of 4% blood cell suspension. The cell suspension was split into 142.5 μL aliquots in 0.2 mL nuclease-free PCR tubes. Stock solutions of **1**−**3**, elaiophylin, and gramicidin were diluted proportionally. Aliquots of 7.5 μL of each stock solution were mixed with the blood suspension. Equal volumes of DMSO and Triton X-100 were used as negative and positive controls, respectively. The mixtures were incubated at 37 °C for 18 h. After incubation, the mixtures were centrifuged at 500*g* for 10 min, and supernatants were measured for hemoglobin absorbance at 540 nm on a microplate reader. The hemolysis rate was calculated using eq 1[58]

$$\text{hemolysis rate} = \frac{OD_{sample} - OD_{negativecontrol}}{OD_{positivecontrol} - OD_{negativecontrol}} \quad (1)$$

Time-Kill Curves

The overnight culture of pathogenic strains (*E. faecium* 36235 and MRSA 718306) was diluted with LB medium to an OD_{600} of 0.4. 40 μL of the diluted bacterial cultures were inoculated into 4 mL of LB liquid medium to achieve an initial concentration of about 5×10^6 CFU/mL. The bacteria were then challenged with the 2×, 4×, and 8× MIC of antarmycin A and cultured at 37 °C and 200 rpm. 200 μL aliquots were removed at the assigned time points (0, 0.5, 1, 2, 4, 8, 12, and 24 h), and CFU/mL was determined by plating the culture onto LB agar in serial dilution. After growth at 37 °C for 24 h, colonies were counted. Experiments were performed three independent times (n = 3).

Mouse Intestinal Infection Model

A single clone of the multidrug-resistant *E. faecium* strain 36235 was grown in 20 mL of LB media at 37 °C with shaking to an OD_{600} of 0.6−0.8. The bacterial cultures were centrifuged, and the cells were washed and resuspended with PBS buffer to a concentration of 1×10^{10} CFUs/mL. Six-week-old C57 female mice were first fed with water supplemented with 5 mg/L metronidazole, vancomycin, and kanamycin for 1 week and then fed with water for 1 day. Then the immune-compromised mice were infected intragastrically with 200 μL of bacterial suspension (2×10^9 CFUs per mouse). At 1 d postinfection, mice were treated intragastrically with antarmycin A at a dose of 60 mg/kg once a day for 3 days. Infection control mice were dosed with vehicle (20% solutol HS-15, 0.2% tween 80, saline) or gentamicin (at a dose of 60 mg/kg). At 5 days postinfection, mice were humanely euthanized. The intestine tissue was aseptically removed; half of the intestine tissue was preserved in 4% formaldehyde fixation solution for histopathological analyses; the rest of the intestine tissue was homogenized, serially diluted, and plated on LB agar for CFU titers. In addition, the weight changes of mice were recorded 1, 2, 3, 4, and 5 d postinfection.

Mouse Epicutaneous Infection Model

A single clone of MRSA USA300 was grown in 20 mL of LB media at 37 °C with shaking to an OD_{600} of 0.6−0.8. The bacterial cultures were centrifuged, and the cells were washed and resuspended with PBS buffer to a concentration of 3×10^9 CFUs/mL. 8 week-old BALB/C female mice first were anesthetized with 1% sodium pentobarbital and then infected intradermally with 50 μL of the bacterial suspension (1.5×10^8 CFUs). At 2 d postinfection, the mice were randomly separated into five groups based on the treatment to be received; each group contained 12 mice. The mice in the first and second group were treated with antarmycin A at doses of 5 and 15 mg/kg per day administered intradermally at the infection sites given twice a day (at 10 h intervals) for 3 days. Mice in the third and fourth groups were set as infection controls and dosed with the vehicle (20% solutol HS-15, 0.2% tween 80, saline) or fusidic acid administered at a dose of 40 mg/kg. Mice in the fifth group were left untreated. At 6 d postinfection, six mice from each group were humanely euthanized and the skin tissues at the infection sites were aseptically removed. Half of the removed skin tissues were preserved in 4% formaldehyde fixation solution for histopathological analyses; the rest of the skin tissues were homogenized, serially diluted, and plated onto LB agar for CFU titers. To further evaluate the postdrug development, the remaining 6 mice in each group were humanely euthanized at 15 d postinfection; the skin tissues at the infection sites were aseptically removed and homogenized, serially diluted, and plated onto LB agar for CFU quantitation. To assess the healing of the infection sites, the wound areas of mice in each group were measured and photographed; the wound areas were calculated with ImageJ software and the data were processed and analyzed with Graphpad 7.0. To evaluate the influence of antarmycin A on the weight of mice, mice in each group were weighed at 3, 6, 9, 12, and 15 d postinfection.

Resistance Studies

For raising resistant mutants by direct plating, a single colony of *S. aureus* ATCC 29213 was inoculated in 5 mL of LB broth and cultured overnight at 37 °C. The overnight culture was diluted with fresh LB to 10^{10} CFUs/mL. 100 μL of the diluted culture was then plated onto an LB plate containing either 4×, 8×, or 16× the MIC of antarmycin A. After 48 h of incubation at 37 °C, no colonies with increasing MIC were detected. For raising a resistant mutant by serial passage, a single colony of *S. aureus* ATCC 29213 was inoculated in 5 mL of LB broth and cultured overnight at 37 °C. The overnight culture was then diluted 1:5000 into fresh LB. 50 μL aliquots of diluted cells were transferred into individual wells of 96-well plates containing 50 μL of serially diluted compound **1**. Plates were statically incubated at 37 °C. After 24 h, the MIC was recorded. For the next round of assays, the cultures in the well with the second highest antibiotic concentration

https://doi.org/10.1021/jacsau.4c00912
JACS Au 2025, 5, 237−249

that showed cloudy growth were selected and diluted 1:5000 into fresh LB. The diluted cells were inoculated to the 96-well plate with serial diluted compound **1**. The MIC was determined as described above. This process was repeated every day for 24 days (3 repeated experiments were used in all experiments).

Membrane Depolarization Assays

The overnight cultures of *S. aureus* ATCC 29213 were harvested and washed with HEPES buffer twice, then resuspended in HEPES to an OD_{600} of 0.5−0.6. The cell suspension was diluted 50 times, and the diluted cells (1 mL) and 10 μL of 4 μM $DiSC_3(5)$ were premixed and incubated at room temperature for 15 min. 50 μL of this mixture was then transferred to each well of black 96-well flat bottom microtiter plates. The initial fluorescence intensity of each well was recorded with a Synergy H1 (excitation/emission = 620/670 nm) at 9 s intervals for 15 min. 50 μL of each compound solution (16 μg/mL compound **1**, 256 μg/mL compound **2**, 4 μg/mL compound **3**, 256 μg/mL compound **1a**, and 4 μg/mL elaiophylin) was added to each well. DMSO was used as vehicle control. Triton-100X (0.5%) and gramicidin (30 μM) were used as positive controls. The fluorescence intensity of each well was then monitored every 9 s for 15 min and plotted by Origin 2021. All tests were biological triple replicates (n = 3).

Cell Lysis Assay. The overnight cultures of *S. aureus* ATCC 29213 were harvested and washed with HEPES buffer twice, then resuspended in HEPES to an OD_{600} of 0.35. Cell suspension (900 μL) and 100 μL of 4 μM SYTOX were premixed and incubated at room temperature for 15 min. 50 μL of this mixture was then transferred to each well of black 96-well flat bottom microtiter plates. The initial fluorescence intensity of each well was recorded with a Synergy H1 (excitation/emission = 488/523 nm) at 9 s intervals for 15 min. The following procedures for the addition of the compound solution and the monitoring of the fluorescence intensity were the same as that for membrane depolarization assays.

Phospholipid Feeding Assay

Each of the tested phospholipids (including phosphatidylglycerol, phosphatidylethanolamine, cardiolipin, lecithin, and distearoyl lecithin) and compound **1** were first codried at molar ratios from 0× to 5×, at 0.5× increments. After drying, the codrying mixtures were resuspended in a small amount of methanol and then in 100 μL of fresh LB to bring the compound to 128 μg/mL. 50 μL of this solution was transferred to a 96-well plate and serially diluted 2 times in LB medium from 128 to 0.012 μg/mL. Overnight cultures of *S. aureus* were diluted to an OD_{600} of 0.1, and this diluted culture was further diluted 100 times in fresh LB medium. 50 μL of diluted bacterial solution was then added to each well, and the final volume of each well was 100 μL. Final assayed concentrations of compound **1** ranged from 64 to 0.06 μg/mL. Based on visual observation, after 16 h of static culture at 37 °C, MIC values were recorded as the lowest concentration with no bacterial growth. All experiments were triplicated (n = 3) and repeated three times (n = 3).

ITC Assay

PG, CL, and PE were each dissolved in sterile water containing 5% DMSO to a final concentration of 2 mM. Compounds **1** and **3** were also each dissolved in the same solution to a final concentration of 0.2 mM. Each of PG/CL/PE was slowly injected into the calorimetric cell filled with compounds **1** or **3**. The injections were repeated 25 times with equilibration intervals of 150 s. The data obtained were analyzed using the instrument software to calculate the equilibrium dissociation constant (K_D), stoichiometry (n), and variations of entropy (ΔS) and enthalpy (ΔH).

■ ASSOCIATED CONTENT

Supporting Information

The Supporting Information is available free of charge at https://pubs.acs.org/doi/10.1021/jacsau.4c00912.

General experimental procedures, fermentation, isolation and structural elucidation of compounds, detailed confirmatory data, and NMR spectra (PDF)

■ AUTHOR INFORMATION

Corresponding Authors

Qinglian Li − *CAS Key Laboratory of Tropical Marine Bio-resources and Ecology, Guangdong Key Laboratory of Marine Materia Medica, South China Sea Institute of Oceanology, Chinese Academy of Sciences, Guangzhou 510301, China;* orcid.org/0000-0002-4052-9801; Phone: +86-20-3406-6449; Email: liql@scsio.ac.cn

Jianhua Ju − *CAS Key Laboratory of Tropical Marine Bio-resources and Ecology, Guangdong Key Laboratory of Marine Materia Medica, South China Sea Institute of Oceanology, Chinese Academy of Sciences, Guangzhou 510301, China; Key Laboratory of Chemical Biology (Ministry of Education), Shandong Basic Science Research Center (Pharmacy), School of Pharmaceutical Sciences, Cheeloo College of Medicine, Shandong University, Jinan 250012, China;* orcid.org/0000-0001-7712-8027; Phone: +86-20-8902-3028; Email: jju@scsio.ac.cn

Authors

Zhenbin Zhou − *CAS Key Laboratory of Tropical Marine Bio-resources and Ecology, Guangdong Key Laboratory of Marine Materia Medica, South China Sea Institute of Oceanology, Chinese Academy of Sciences, Guangzhou 510301, China; College of Oceanology, University of Chinese Academy of Sciences, Qingdao 266400, China*

Jiafan Yang − *CAS Key Laboratory of Tropical Marine Bio-resources and Ecology, Guangdong Key Laboratory of Marine Materia Medica, South China Sea Institute of Oceanology, Chinese Academy of Sciences, Guangzhou 510301, China; College of Oceanology, University of Chinese Academy of Sciences, Qingdao 266400, China;* orcid.org/0000-0001-5703-0890

Junying Ma − *CAS Key Laboratory of Tropical Marine Bio-resources and Ecology, Guangdong Key Laboratory of Marine Materia Medica, South China Sea Institute of Oceanology, Chinese Academy of Sciences, Guangzhou 510301, China;* orcid.org/0000-0002-0641-7291

Zhuo Shang − *Key Laboratory of Chemical Biology (Ministry of Education), Shandong Basic Science Research Center (Pharmacy), School of Pharmaceutical Sciences, Cheeloo College of Medicine, Shandong University, Jinan 250012, China*

Runping Fang − *Key Laboratory of Chemical Biology (Ministry of Education), Shandong Basic Science Research Center (Pharmacy), School of Pharmaceutical Sciences, Cheeloo College of Medicine, Shandong University, Jinan 250012, China*

Xinpeng Tian − *CAS Key Laboratory of Tropical Marine Bio-resources and Ecology, Guangdong Key Laboratory of Marine Materia Medica, South China Sea Institute of Oceanology, Chinese Academy of Sciences, Guangzhou 510301, China*

Complete contact information is available at: https://pubs.acs.org/10.1021/jacsau.4c00912

https://doi.org/10.1021/jacsau.4c00912
JACS Au 2025, 5, 237−249

Author Contributions

Z.Z., Q.L., and J.J. designed the research; Z.Z., J.Y., and R.F. performed the research; Z.Z., J.M., Z.S., X.T., and Q.L. analyzed the data; Z.Z., Q.L., and J.J. wrote the manuscript.

Notes

The authors declare no competing financial interest.

■ ACKNOWLEDGMENTS

This work was supported in part by the National Natural Science Foundation of China (22037006, U2106207, U23A20107, and 82022067), the Guangdong Local Innovation Team Program (2019BT02Y262), the Natural Science Foundation of Guangdong (2021B1515020036 and 2023B1515120053), the National Key Research and Development Program of China (2022YFC2804100 and 2023YFA0914200), the Open Program of Shenzhen Bay Laboratory (SZBL2021080601006), and the Nansha District Science and Technology Plan Project (NSJL202102). We thank Professor Jianhua Liu from South China Agricultural University, Professor Minggui Wang from Huashang Hospital, and Professor Naiqi Huang from The Third RenMin Hospital of Shenzhen for the gifts of pathogenic bacteria.

■ REFERENCES

(1) Goldberg, J.; Clezy, K.; Jasovský, D.; Uyen-Cateriano, A. Leaving no one behind: the need for a truly global response to antimicrobial resistance. *Lancet Microbe* **2022**, *3*, e2−e3.
(2) Ventola, C. L. The antibiotic resistance crisis: part 1: causes and threats. *P. T.* **2015**, *40*, 277−283.
(3) Lancet, T. Antimicrobial resistance: time to repurpose the Global Fund. *Lancet* **2022**, *399*, 335.
(4) Murray, C. J. L.; Ikuta, K. S.; Sharara, F.; Swetschinski, L.; Robles Aguilar, G.; Gray, A.; Han, C.; Bisignano, C.; Rao, P.; Wool, E.; et al. Global burden of bacterial antimicrobial resistance in 2019: a systematic analysis. *Lancet* **2022**, *399*, 629−655.
(5) World Health Organization. *WHO Bacterial Priority Pathogens List 2024: Bacterial Pathogens of Public Health Importance to Guide Research, Development and Strategies to Prevent and Control Antimicrobial Resistance*; World Health Organization, 2024. https://www.who.int/publications/i/item/9789240093461.(accessed 2024−05−17).
(6) Tillotson, G. A crucial list of pathogens. *Lancet Infect. Dis.* **2018**, *18*, 234−236.
(7) Van Tyne, D.; Gilmore, M. S. Friend turned foe: evolution of enterococcal virulence and antibiotic resistance. *Annu. Rev. Microbiol.* **2014**, *68*, 337−356.
(8) Miller, W. R.; Murray, B. E.; Rice, L. B.; Arias, C. A. Vancomycin-resistant enterococci: therapeutic challenges in the 21st century. *Infect. Dis. Clin. North. Am.* **2016**, *30*, 415−439.
(9) Gilmore, M.; Lebreton, S. F.; Schaik, V. W. Genomic transition of enterococci from gut commensals to leading causes of multidrug-resistant hospital infection in the antibiotic era. *Curr. Opin. microbiol.* **2013**, *16*, 10−16.
(10) van Hal, S. J.; Willems, R. J. L.; Gouliouris, T.; Ballard, S. A. T.; Coque, M.; Hammerum, A. M.; Hegstad, K.; Westh, H. T.; Howden, B. P.; Malhotra-Kumar, S.; et al. The global dissemination of hospital clones of *Enterococcus faecium*. *Genome Med.* **2021**, *13*, 52−12.
(11) Reinseth, I. S.; Ovchinnikov, K. V.; Tønnesen, H. H.; Carlsen, H.; Diep, D. B. The increasing issue of vancomycin-resistant enterococci and the bacteriocin solution. *Probiotics antimicrobi. Proteins* **2020**, *12*, 1203−1217.
(12) Gouliouris, T.; Coll, F.; Ludden, C.; Blane, B.; Raven, K. E.; Naydenova, P.; Crawley, C.; Török, M. E.; Enoch, D. A.; Brown, N. M. E.; et al. Quantifying acquisition and transmission of *Enterococcus faecium* using genomic surveillance. *Nat. microbiol.* **2021**, *6*, 103−111.
(13) Arias, C. A.; Murray, B. E. The rise of the *enterococcus*: beyond vancomycin resistance. *Nat. Rev. Microbiol.* **2012**, *10*, 266.
(14) Zhou, X.; Willems, R. J. L.; Friedrich, A. W.; Rossen, J. W. A.; Bathoorn, E. *Enterococcus faecium*: from microbiological insights to practical recommendations for infection control and diagnostics. *Antimicrob. Resist. Infect. Control* **2020**, *9*, 130.
(15) Cheung, G. Y. C.; Bae, J. S.; Otto, M. Pathogenicity and virulence of *Staphylococcus aureus*. *Virulence* **2021**, *12*, 547−569.
(16) Lee, A. S.; de Lencastre, H.; Garau, J.; Kluytmans, J.; Malhotra-Kumar, S.; Peschel, A.; Harbarth, S. Methicillin-resistant *Staphylococcus aureus*. *Nat. rev. Dis. primers* **2018**, *4*, 18033−18123.
(17) Grinberg, A.; Biggs, P. J.; Zhang, J.; Ritchie, S.; Oneroa, Z.; O'Neill, C.; Karkaba, A.; Velathanthiri, N. S.; Coombs, G. W. Genomic epidemiology of methicillin-susceptible *Staphylococcus aureus* across colonisation and skin and soft tissue infection. *J. Infect.* **2017**, *75*, 326−335.
(18) Jacobs, D. M.; Shaver, A. Prevalence of and outcomes from *Staphylococcus aureus* pneumonia among hospitalized patients in the United States, 2009−2012. *Am. J. Infect. Control* **2017**, *45*, 404−409.
(19) Kourtis, A. P.; Hatfield, K.; Baggs, J.; Mu, Y.; See, I.; Epson, E.; Nadle, J.; Kainer, M. A.; Dumyati, G.; Petit, S.; et al. Vital signs: epidemiology and recent trends in methicillin-resistant and in methicillin-susceptible *Staphylococcus aureus* bloodstream infections−United States *MMWR Morb. Mortal. Wkly. Rep.* **2019**, *68*, 214−219.
(20) Kavanagh, K. T. Control of MSSA and MRSA in the United States: protocols, policies, risk adjustment and excuses. *Antimicrob. Resist. Infect. Control* **2019**, *8*, 103−108.
(21) Piddock, L. J. The crisis of no new antibiotics—what is the way forward? *Lancet infect. Dis.* **2012**, *12*, 249−253.
(22) Kwon, J. H.; Powderly, W. G. The post-antibiotic era is here. *Science* **2021**, *373*, 471.
(23) Cook, M. A.; Wright, G. D. The past, present, and future of antibiotics. *Sci. Transl. Med.* **2022**, *14*, No. eabo7793.
(24) Nathan, C. Resisting antimicrobial resistance. *Nat. Rev. Microbiol.* **2020**, *18*, 259−260.
(25) Miethke, M.; Pieroni, M.; Weber, T.; Brönstrup, M.; Hammann, P.; Halby, L.; Arimondo, P. B.; Glaser, P.; Aigle, B.; et al. Towards the sustainable discovery and development of new antibiotics. *Nat. Rev. Chem* **2021**, *5*, 726−749.
(26) Shen, B. A new golden age of natural products drug discovery. *Cell* **2015**, *163*, 1297−1300.
(27) Barnes, E. C.; Kumar, R.; Davis, R. A. The use of isolated natural products as scaffolds for the generation of chemically diverse screening libraries for drug discovery. *Nat. Prod. Rep.* **2016**, *33*, 372−381.
(28) Wright, G. D. Opportunities for natural products in 21st century antibiotic discovery. *Nat. Prod. Rep.* **2017**, *34*, 694−701.
(29) Chen, J. W.; Jia, Y. Y.; Sun, Y.; Liu, K.; Zhou, C. H.; Liu, C.; Li, D. H.; Liu, G. L.; Zhang, C. S.; Yang, T.; et al. Global marine microbial diversity and its potential in bioprospecting. *Nature* **2024**, *633*, 371−379.
(30) Stonik, V. A.; Makarieva, T. N.; Shubina, L. K. Antibiotics from Marine Bacteria. *Biochemistry (Mosc)* **2020**, *85*, 1362−1373.
(31) Chen, B.; Yang, Y.; Liang, X.; Yu, K.; Zhang, T.; Li, X. Metagenomic profiles of antibiotic resistance genes (ARGs) between human impacted estuary and deep ocean sediments. *Environ. Sci. Technol.* **2013**, *47*, 12753−12760.
(32) Brown, E. D.; Wright, G. D. Antibacterial drug discovery in the resistance era. *Nature* **2016**, *529*, 336−343.
(33) Panter, F.; Bader, C. D.; Müller, R. The sandarazols are cryptic and structurally unique plasmid-encoded toxins from a rare Myxobacterium. *Angew. Chem., Int. Ed. Engl.* **2021**, *60*, 8081−8088.
(34) Van Arnam, E. B.; Ruzzini, A. C.; Sit, C. S.; Horn, H.; Pinto-Tomás, A. A.; Currie, C. R.; Clardy, J. Selvamicin, an atypical antifungal polyene from two alternative genomic contexts. *Proc. Natl. Acad. Sci. U.S.A.* **2016**, *113*, 12940−12945.

(35) Van Arnam, E. B.; Ruzzini, A. C.; Sit, C. S.; Currie, C. R.; Clardy, J. A rebeccamycin analog provides plasmid-encoded niche defense. *J. Am. Chem. Soc.* **2015**, *137*, 14272−14274.
(36) Arcamone, F.; Bertazzoli, C.; Ghione, M.; Scotti, T. Melanosporin and elaiophylin, new antibiotics from *Streptomyces melanosporus* n. sp. G. *Microbiol* **1959**, *7*, 207−216.
(37) Gui, M.; Zhang, M.; Wu, W.; Sun, P. Natural occurrence, bioactivity and biosynthesis of eaiophylin analogues. *Molecules* **2019**, *24*, 3840.
(38) Yoon, S. H.; Ha, S. M.; Lim, J.; Kwon, S.; Chun, J. A large-scale evaluation of algorithms to calculate average nucleotide identity. *Antonie Van Leeuwenhoek* **2017**, *110*, 1281−1286.
(39) Netolitzky, D. J.; Wu, X.; Jensen, S. E.; Roy, K. L. Giant linear plasmids of *β*-lactam antibiotic producing *Streptomyces*. *FEMS microbial. Lett.* **1995**, *131*, 27−34.
(40) Kinashi, H.; Shimaji, M.; Sakai, A. Giant linear plasmids in *Streptomyces* which code for antibiotic biosynthesis genes. *Nature* **1987**, *328*, 454−456.
(41) Gust, B.; Challis, G. L.; Fowler, K.; Kieser, T.; Chater, K. F. PCR-targeted Streptomyces gene replacement identifies a protein domain needed for biosynthesis of the sesquiterpene soil odor geosmin. *Proc. Natl. Acad. Sci. U.S.A.* **2003**, *100*, 1541−1546.
(42) Bilyk, O.; Oliveira, G. S.; de Angelo, R. M.; Almeida, M. O.; Honorio, K. M.; Leeper, F. J.; Dias, M. V.; Leadlay, P. F. Enzyme-catalyzed spiroacetal formation in polyketide antibiotic biosynthesis. *J. Am. Chem. Soc.* **2022**, *144*, 14555−14563.
(43) Singh, A. A.; Rowley, J. A.; Schwartz, B. D.; Kitching, W.; De Voss, J. J. Oxidative carbon-carbon bond cleavage is a key step in spiroacetal biosynthesis in the fruit fly *Bactrocera cacuminata*. *J. Org. Chem.* **2014**, *79*, 7799−7821.
(44) Xie, Y.; Ma, J.; Qin, X.; Li, Q.; Ju, J. Identification and utilization of two important transporters: SgvT1 and SgvT2, for griseoviridin and viridogrisein biosynthesis in *Streptomyces griseoviridis*. *Microb. cell fact.* **2017**, *16*, 177−210.
(45) Ikeno, S.; Yamane, Y.; Ohishi, Y.; Kinoshita, N.; Hamada, M.; Tsuchiya, K. S.; Hori, M. ABC transporter genes, kasKLM, responsible for self-resistance of a kasugamycin producer strain. *J. Antibiot.* **2000**, *53*, 373−384.
(46) Williams, D. H.; Maguire, A. J.; Tsuzuki, W.; Westwell, M. S. An analysis of the origins of a cooperative binding energy of dimerization. *Science* **1998**, *280*, 711−714.
(47) Chen, H.; Thomas, M. G.; Hubbard, B. K.; Losey, H. C.; Walsh, C. T.; Burkart, M. D. Deoxysugars in glycopeptide antibiotics: enzymatic synthesis of TDP-l-epivancosamine in chloroeremomycin biosynthesis. *Proc. Natl. Acad. Sci. U.S.A.* **2000**, *97*, 11942−11947.
(48) Nakayama, A.; Okano, A.; Feng, Y.; Collins, J. C.; Collins, K. C.; Walsh, C. T.; Boger, D. L. Enzymatic glycosylation of vancomycin aglycon: completion of a total synthesis of vancomycin and N- and C-Terminus substituent effects of the aglycon substrate. *Org. Lett.* **2014**, *16*, 3572−3575.
(49) Xu, L.; Huang, H.; Wei, W.; Zhong, Y.; Tang, B.; Yuan, H.; Zhu, L.; Huang, W.; Ge, M.; Yang, S.; Zheng, H.; et al. Complete genome sequence and comparative genomic analyses of the vancomycin-producing *Amycolatopsis orientalis*. *BMC Genomics* **2014**, *15*, 363−418.
(50) Namikawa, K.; Tanaka, N.; Ota, Y.; Takamatsu, M.; Kosugi, M.; Tokai, Y.; Yoshimizu, S.; Horiuchi, Y.; Ishiyama, A.; Yoshio, T.; Hirasawa, T.; et al. Genomic features of Helicobacter pylori-naïve diffuse-type gastric cancer. *J. Pathol* **2022**, *258*, 300−311.
(51) Kumagai, K.; Shimizu, T.; Nikaido, M.; Hirano, T.; Kakiuchi, N.; Takeuchi, Y.; Minamiguchi, S.; Sakurai, T.; Teramura, M.; Utsumi, T.; Hiramatsu, Y.; et al. On the origin of gastric tumours: analysis of a case with intramucosal gastric carcinoma and oxyntic gland adenoma. *J. Pathol.* **2023**, *259*, 362−368.
(52) Suzuki, H.; Matsuzaki, J. Gastric cancer: evidence boosts Helicobacter pylori eradication. *Nat. Rev. Gastroenterol. Hepatol.* **2018**, *15*, 458−460.
(53) Zhang, H.; Chen, Y.; Li, Y.; Song, Y.; Ma, J.; Ju, J. Secondary metabolites and biosynthetic gene clusters analysis of deep-sea hydrothermal vent-derived *Streptomyces* sp. SCSIO ZS0520. *Mar. Drugs* **2022**, *20*, 393.
(54) Song, M.; Liu, Y.; Li, T.; Liu, X.; Hao, Z.; Ding, S.; Panichayupakaranant, P.; Zhu, K.; Shen, J. Plant natural flavonoids against multidrug resistant pathogens. *Adv. Sci.* **2021**, *8*, 2100749.
(55) Yang, R.; Hou, E.; Cheng, W.; Yan, X.; Zhang, T.; Li, S.; Yao, H.; Liu, J.; Guo, Y. Membrane-targeting neolignan-antimicrobial peptide mimic conjugates to combat methicillin-resistant *Staphylococcus aureus* (MRSA) infections. *J. Med. Chem.* **2022**, *65*, 16879−16892.
(56) Li, Q.; Ding, W.; Yao, Z.; Tu, J.; Wang, L.; Huang, H.; Li, S.; Ju, J. AbmV catalyzes tandem ether installation and hydroxylation during neoabyssomicin/abyssomicin biosynthesis. *Org. Lett.* **2018**, *20*, 4854.
(57) CLSI *Methods for Dilution Antimicrobial Susceptibility Tests for Bacteria that Grow Aerobically. Approved Standard-11th Ed*; Clinical and Laboratory Standards Institute, 2018; p M07
(58) Ren, H.; Dommaraju, S. R.; Huang, C.; Cui, H.; Pan, Y.; Nesic, M.; Zhu, L.; Sarlah, D.; Mitchell, D. A.; Zhao, H. Genome mining unveils a class of ribosomal peptides with two amino termini. *Nat. Commun.* **2023**, *14*, 1624.

https://doi.org/10.1021/jacsau.4c00912
JACS Au 2025, 5, 237−249